Available online at www.sciencedirect.com

ScienceDirect

www.elsevier.com/locate/jes

JES JOURNAL OF ENVIRONMENTAL SCIENCES

www.jesc.ac.cn

Research Article

Blockage of ATPase-mediated energy supply inducing metabolic disturbances in algal cells under silver nanoparticles stress

Ruohua Qu[1], *Mi Chen*[1], *Jingfu Liu*[2], *Qiting Xie*[1], *Na Liu*[1], *Fei Ge*[1,*]

[1] *Department of Environment, College of Environment and Resources, Xiangtan University, Xiangtan 411105, China.*
[2] *State Key Laboratory of Environmental Chemistry and Ecotoxicology, Research Center for Eco-Environmental Sciences, Chinese Academy of Sciences, Beijing 100085, China*

ARTICLE INFO

Article history:
Received 14 August 2022
Revised 12 October 2022
Accepted 17 October 2022
Available online 30 October 2022

Keywords:
Adenosine triphosphate
Metabolomics
Molecular dynamics simulations
Nanoparticles
Algae

ABSTRACT

Adenosine triphosphate (ATP) generation of aquatic organisms is often subject to nanoparticles (NPs) stress, involving extensive reprogramming of gene expression and changes in enzyme activity accompanied by metabolic disturbances. However, little is known about the mechanism of energy supply by ATP to regulate the metabolism of aquatic organisms under NPs stress. Here, we selected extensively existing silver nanoparticles (AgNPs) to investigate their implications on ATP generation and relevant metabolic pathways in alga (*Chlorella vulgaris*). Results showed that ATP content significantly decreased by 94.2% of the control (without AgNPs) in the algal cells at 0.20 mg/L AgNPs, which was mainly attributed to the reduction of chloroplast ATPase activity (81.4%) and the downregulation of ATPase-coding genes *atp*B and *atp*H (74.5%-82.8%) in chloroplast. Molecular dynamics simulations demonstrated that AgNPs competed with the binding sites of substrates adenosine diphosphate and inorganic phosphate by forming a stable complex with ATPase subunit beta, potentially resulting in the reduced binding efficiency of substrates. Furthermore, metabolomics analysis proved that the ATP content positively correlated with the content of most differential metabolites such as D-talose, myo-inositol, and L-allothreonine. AgNPs remarkably inhibited ATP-involving metabolic pathways, including inositol phosphate metabolism, phosphatidylinositol signaling system, glycerophospholipid metabolism, aminoacyl-tRNA biosynthesis, and glutathione metabolism. These results could provide a deep understanding of energy supply in regulating metabolic disturbances under NPs stress.

Introduction

For all organisms, life continuation is inseparable from energy metabolism (Chen et al., 2015b; Jin et al., 2019; Liang et al., 2022). Photophosphorylation, oxidative phosphorylation, and citrate cycle are crucial energy metabolism, which provides all of the energy product adenosine triphosphate (ATP) for the anabolism and catabolism of organisms (Chu et al., 2020;

* Corresponding author.
E-mail: gefei@xtu.edu.cn (F. Ge).

https://doi.org/10.1016/j.jes.2022.10.029
1001-0742/

Middepogu et al., 2018; Tao et al., 2020; Wang et al., 2021). However, these processes are often subject to various xenobiotic pollutant stresses, such as nanoparticles (NPs), resulting in the imbalance of the energy regulation network (Cao et al., 2021; Luo et al., 2021; Qi et al., 2022). The blockage of ATP supply would inevitably limit energy-required activities in organisms, accompanied by various metabolic disturbances (Liu et al., 2021; Liu and Zhu, 2020; Matich et al., 2019; Zhong et al., 2019). These metabolic disturbances might manifest in the alteration of metabolites involved in energy storage and consumption, such as the reduction of fatty acids, carbohydrates, etc. (Mo et al., 2023; Zhang et al., 2020b; Zhong et al., 2019). Nonetheless, relatively little information is available regarding the mechanism of energy supply by ATP to regulate the metabolism of aquatic organisms under NPs stress at a molecular level.

Generally, the perturbations of ATP generation by NPs can be attributed to oxidative damage to mitochondria and chloroplasts, changes in enzyme activity, and extensive reprogramming of related gene expression (Chen et al., 2019; Costa et al., 2016; Marisa et al., 2022). Recently, most research focused on the mechanism of ATP generation in mitochondria, such as the alteration of transcriptional levels of phosphoenolpyruvate carboxykinase, succinyl-CoA synthetase, and so on (Luo et al., 2021). Aside from these, ATPase in the chloroplast is also a key enzyme that can catalyze the conversion of inorganic phosphate (Pi) and adenosine diphosphate (ADP) to ATP (Middepogu et al., 2018). It was found that titanium dioxide nanoparticles (TiO_2 NPs) could decrease the activity of ATPase in the chloroplast to reduce the ATP content of *Chlorella pyrenoidosa*, while no significant effects were found for the expression level of ATPase gene in the chloroplast (Middepogu et al., 2018). Differently, exposure to TiO_2 NPs upregulated the transcriptional levels of ATPase genes in the chloroplast of *Synechocystis* sp. (Wu et al., 2018). From these, the changes in ATPase activity in the chloroplast may be regulated by other processes in addition to the reprogramming of related gene expression. However, comprehensive research remains limited on the mechanisms of NPs to disturb ATP generation by regulating the ATPase in the chloroplast. Therefore, it warrants advanced investigation into the underlying mechanisms.

Silver nanoparticles (AgNPs) are the most commonly applied nanomaterials due to their excellent antibacterial, antiviral and antifungal properties (Grün et al., 2018; Guo et al., 2018; Huang et al., 2019). Such widespread use inevitably caused the sustained release of AgNPs into aquatic ecosystems, raising concerns about the potential toxicity to aquatic biota (Huang et al., 2020; Liu et al., 2020b; Nam et al., 2018; Wang et al., 2019). However, key knowledge gaps remain on how AgNPs affect energy supply by ATP in the chloroplast to regulate the metabolism of aquatic organisms. *Chlorella vulgaris* (*C. vulgaris*) is an ecologically significant primary producer in aquatic ecosystems, which is often used as an ecotoxicological model. Our previous study found its sensitivity to NPs (Liu et al., 2018; Zhao et al., 2019). Therefore, this study selected *C. vulgaris* as the research object and explored its mechanism of ATP generation and relevant metabolic pathways in response to AgNPs stress. The objectives were to (1) investigate the effect of AgNPs on algal growth and ATP generation, (2) clarify the mechanism of ATP generation in response to AgNPs stress by quantitative real-time PCR analysis and molecular dynamics simulations, and (3) identify the ATP-involving metabolic pathways influenced by AgNPs using non-target metabolomics. This study helps us better understand the implication of AgNPs on the energy metabolism of aquatic organisms.

1. Materials and methods

1.1. Chemicals

AgNPs (CAS no.7440-22-4) with a diameter of 15 ± 5 nm were acquired from Xianfeng Nano Material Technology Co., Ltd. (Nanjing, China). The detailed physic-chemical characterizations of AgNPs were presented in Supporting Information Appendix A **Text S1** and **Fig. S1** (Xie et al., 2022). Phenylmethane sulfonyl fluoride (PMSF, CAS no. 329-98-6, purity > 98%) was obtained from Aladdin Industrial Co., Ltd. (Shanghai, China). Reagent bis (trimethylsilyl) trifluoroacetamide (with 1% TMCS, *V/V*) was acquired from Regis Technologies, Inc. (Morton Grove, USA). All other solvents and reagents were supplied by China National Medicines Co., Ltd. (Beijing, China).

1.2. Algal cultivation and growth

C. vulgaris (FACHB-1068) was purchased from the Freshwater Algal Culture Collection at the Institute of Hydrobiology (Chinese Academy of Science, Wuhan, China). It was maintained in a stable growing condition in fresh OECD medium according to guideline 201 of Organization for Economic Cooperation and Development (OECD, 2006). The detailed composition of OECD medium is presented in Supporting Information Appendix A **Table S1**. Algae were pre-cultured in temperature-controlled illumination incubators (GDN, Ningbo Dongnan Instrument Co., Ltd., China) at constant temperature (25°C) with a light/dark cycle (12 hr/12 hr) under 2500 lux illumination (Chen et al., 2015a). After being cultivated in the logarithmic growth phase, the algal cells were obtained by centrifugation (4°C, 4000 ×*g*, 10 min) and then inoculated in Erlenmeyer flasks (250 mL) containing 100 mL of OECD medium. Subsequently, the fresh stock solution of AgNPs was added to the culture medium of *C. vulgaris* to make final concentrations of 0, 0.05, 0.10, 0.15, and 0.20 mg/L, respectively. The concentrations of AgNPs were chosen based on the 96-hr EC_{50} of AgNPs to *C. vulgaris* (0.13 mg/L). To evaluate the effect of dissolved Ag on algal growth, algal cultures were exposed to 0, 2.3, and 9.5 μg/L Ag^+, respectively. The concentrations of Ag^+ correspond to the dissolved Ag in the suspensions of 0.05 and 0.20 mg/L AgNPs. The primary algal cell density was maintained at 3.5×10^5 cells/mL. The algal biomass was obtained by determining the optical density at a wavelength of 680 nm using a spectrophotometer (V1000 spectrophotometer, Shanghai AOE Instrument Co., Ltd., China). The relative chlorophyll content was measured as previously stated by Xie et al. (2020). The morphologies of algal cells after exposure to AgNPs for 4 days were monitored with transmission electron microscopy (TEM, JEM2100EX, JEOL, Japan) following the methods presented in Appendix A **Text S2**.

1.3. ATP and ADP detection

After exposure to AgNPs for 7 days, the cell suspension (90 mL) was centrifuged at 4000 ×*g* for 10 min to collect the cells. The collected algal cells were stored at −80°C before analysis. The contents of ATP and ADP in the algal cells were analyzed with an Agilent 1260 infinity high-performance liquid chromatography (HPLC) coupled with a variable wavelength detector and an ODS C18 column (4.6 mm × 250 mm, 5 μm; Agilent Technologies, Santa Clara, CA, USA). In brief, into each sample was added 2 mmol/L of the boiling $MgSO_4$ and the obtained mixture was heated in a boiling water bath for 10 min. After being homogenized mechanically following previous procedures (Zhou et al., 2016), the collected supernatant was measured by HPLC analysis within 2 hr. The supernatant injection volume was twenty μL. A mobile phase consisting of 97.5% KH_2PO_4-K_2HPO_4 buffer (50 mmol/L, containing 1 mmol/L EDTA, pH 6.0) and 2.5% methanol was used at a flow rate of 1.0 mL/min with the column temperature at 25 ± 0.5°C. The distinctly separated peaks of ATP and ADP were measured at 259 nm.

1.4. Measurement of ATPase activity

After exposure to AgNPs for 7 days, the cell suspension (90 mL) was centrifuged at 4000 ×*g* for 10 min. Subsequently, the obtained algal cells were homogenized mechanically in cooled phosphate buffer saline (PBS, pH 7.4). The supernatant was collected centrifugally for test. The H^+-ATPase activity was determined with the manufacturer's instructions of a plant H^+-ATPase ELISA kit (Shanghai Tongwei Biotechnology Co., Ltd., China) using a microplate reader (i-Mark, Bio-Rad, Japan) at a wavelength of 450 nm.

The thylakoid membrane of algal samples was extracted by using the method presented in our previous study (Liu et al., 2020a; Zhang et al., 2019). The detailed information on the method is available in Appendix A **Text S3**. Subsequently, the thylakoid membrane was suspended and incubated with 0.10 mg/L pre-cooling dithiothreitol for 15 min. The chloroplast ATPase activity was determined with the manufacturer's instructions of an ATPase assay kit (Nanjing Jiancheng Bioengineering Institute, China) using the microplate reader at a wavelength of 630 nm. Spearman correlation analysis was performed to assess the possible correlation between chloroplast ATPase activity and ATP content of algal cells.

1.5. Oxidative damage

The ROS assay kit (Beyotime Biotechnology, China) based on 2′,7′-dichlorodihydrofluorescein diacetate (H_2DCFDA) as a fluorescence probe was used to measure ROS production. Moreover, a thiobarbituric acid reactive substances (TBARS) assay was used to analyze malondialdehyde (MDA) content. The experimental details are shown in Appendix A **Text S4**.

1.6. Quantitative real-time PCR analysis

The total RNA of algal cells on the 7th day was collected using an RNA Purification Kit (Beijing Solarbio Science & Technology Co., Ltd., China). The RNA was converted into cDNA using an Hifair 1st Strand cDNA Synthesis Kit (Yeasen biotech Co., Ltd., China). Real-time PCR was conducted using Hieff qPCR SYBR Green Master Mix (Yeasen biotech Co., Ltd., China) on a Roche LightCycler 96 system (Roche Diagnostics, USA). Three ATPase-related genes, including ATPase CF1 beta chain (*atp*B), ATPase CF0 C chain (*atp*H), and ATPase CF0 A chain (*atp*I), were selected for study. PCR primers were designed based on *C. vulgaris* chloroplast DNA sequence using NCBI Database (https://blast.ncbi.nlm.nih.gov/Blast.cgi). The primers of these genes are listed in Appendix A **Table S2**. Relative gene expressions of the tested genes were quantified using the method of comparative $2^{-\Delta\Delta Ct}$. The internal reference gene 18s rRNA was used for normalization.

1.7. Molecular docking and molecular dynamics simulations

To explore the interaction between AgNPs and ATPase subunit beta (AtpB), molecular dynamics simulations were conducted using the GROMACS 2019.6 software (Berendsen et al., 1995). All molecular dynamics simulations were carried out under an isothermal and isostatic ensemble, which were regulated by the V-rescale and Parrinello-Rahman methods (Carretero-González et al., 2005). Additionally, docking calculus was performed using PatchDock server Beta 1.3 version, a molecular docking algorithm based on shape complementarity principles (Schneidman-Duhovny et al., 2005). The detailed parameters of molecular docking and molecular dynamics simulations are presented in Appendix A **Text S5**.

1.8. Metabolic analysis

After exposure to AgNPs for 7 days, the cell suspension (20 mL) was centrifuged at 4000 ×*g* for 10 min. The collected algal cells were rapidly frozen in liquid nitrogen. The metabolites were extracted from the algal samples using a pre-cooling extraction mixture (1 mL, methanol/chloroform (*V*/*V*) =3:1) with adonitol as an internal standard. Metabolites were analyzed by gas chromatography coupled with a time-of-flight mass spectrometer (GC/TOF-MS). The detailed information on the methods and instrument parameters are presented in Appendix A **Text S6**.

For multivariate statistical data analysis, supervised partial least-squares discriminant analysis (PLS-DA) was run via SIMCA-P 13 (Umetrics, Umea, Sweden). Variable importance in projection (VIP) values were gained from the PLS-DA model. In addition, MetaboAnalyst 5.0 (http://www.metaboanalyst.ca/) was applied for biological pathway analysis, univariate one-way analysis of variance (ANOVA), and heatmaps analysis. The *p*-value threshold and impact value threshold calculated for pathway identification were set at 0.01 and 0.1, respectively. The metabolic correlation network was conducted by a network visualization using Gephi version 0.9.2.

1.9. Statistical analysis

All data were expressed as mean ± standard deviation (SD) of triplicates unless otherwise noted. The metabolic analysis was conducted with six replicates. Student *t*-test was

conducted using GraphPad Prism (version 7.0, San Diego, CA, USA). The probabilities of $p < 0.05$ and $p < 0.01$ were defined as significant and highly significant differences, respectively.

2. Results and discussion

2.1. ATP generation inhibited by AgNPs

To estimate the effects of AgNPs on algal growth, we analyzed the biomass and chlorophyll content of algal cells in response to AgNPs stress. As shown in **Fig. 1a**, AgNPs inhibited the algal growth, and the inhibition effects were more noticeable at higher concentrations ($p < 0.05$). When the algal cells were treated with different concentrations of AgNPs for 7 days, the biomass decreased by 18.4%-70.1% of the control (without AgNPs). Similarly, the chlorophyll content was reduced by 5.68%-74.9% of the control (Appendix A **Fig. S2**). Generally, the release of Ag^+ was regarded as one of the main mechanisms of AgNPs toxicity (Zhang et al., 2020a). To explore the effect of dissolved Ag^+ in the AgNPs suspensions on the algal growth, the experiments were performed in the presence of 2.3 and 9.5 μg/L Ag^+. Results showed that Ag^+ slightly decreased algal biomass and did not affect chlorophyll content significantly in Appendix A **Fig. S3**. The inhibition effects of AgNPs were more noticeable than those of Ag^+. These suggested that AgNPs, rather than dissolved Ag^+ in the AgNPs suspensions, contributed to the inhibition of algal growth in this study.

Algal growth is energy-consuming because various biochemical processes, including nutrient uptake, carbon fixation in photosynthesis, aerobic respiration, etc., require energy from ATP hydrolysis. Given the importance of ATP synthesis in algal growth, we further investigated the effects of AgNPs on the contents of ATP and ADP in algal cells. As depicted in **Fig. 1b**, the ATP content declined with the increasing concentration of AgNPs, which significantly decreased by 94.2% of the control under 0.20 mg/L AgNPs stress. Meanwhile, a dramatic decrease in ATP/ADP ratio can be seen in AgNPs-exposed groups, indicating the disruptions in the conversion of ADP and Pi into ATP. Nevertheless, the decomposition of ATP into ADP was also inhibited by AgNPs according to the decreased H^+-ATPase activity ($p < 0.05$, **Fig. 1c**). In particular, the H^+-ATPase activity decreased by 73.0% of the control at 0.20 mg/L AgNPs, suggesting less energy consumption. As is well known, H^+-ATPase uses the energy from ATP hydrolysis to supply a proton concentration gradient for the uptake of nutriment (Liang and Zhang, 2018). However, the energy supply to H^+-ATPase was decreased, thereby causing attenuation of enzyme activity. In general, the storage of ATP in algal cells depends on both the production ability and the consumption amount (Liu et al., 2015). The above result indicated that ATP generation was reduced faster than energy consumption. The blockage of energy supply caused by the inhibited ATP generation may contribute to the significant biomass loss in response to AgNPs stress. Therefore, it is necessary to further explore the mechanism of ATP reduction in algal cells under AgNPs stress.

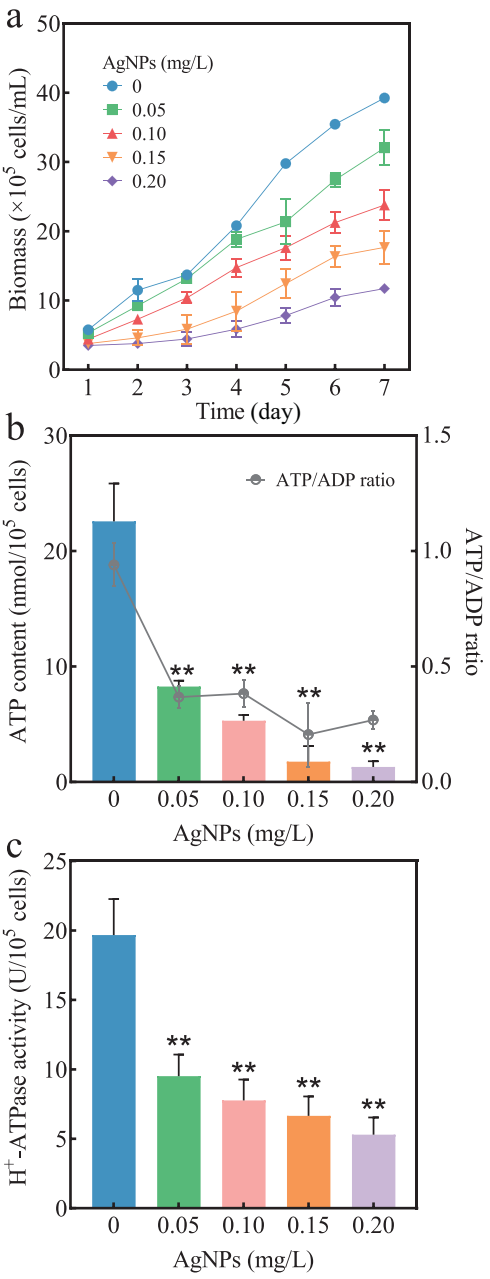

Fig. 1 – The variations of biomass (a), adenosine triphosphate (ATP) content and ATP / adenosine diphosphate (ADP) ratio (b), and H^+-ATPase activity (c) in *C. vulgaris* under AgNPs stress. Data were expressed as mean ± SD ($n = 3$). ** indicates that the values are significantly different compared with the control group ($p < 0.01$).

2.2. Mechanism of ATP reduction under AgNPs stress

Chloroplast ATPase activity. Generally, chloroplasts and mitochondria constitute the most prominent source of ATP production through photophosphorylation and oxidative phosphorylation (Chen et al., 2015b), respectively. However, we observed that the ultrastructure of chloroplast was damaged by AgNPs (Appendix A **Fig. S4**). Thylakoid membranes were dis-

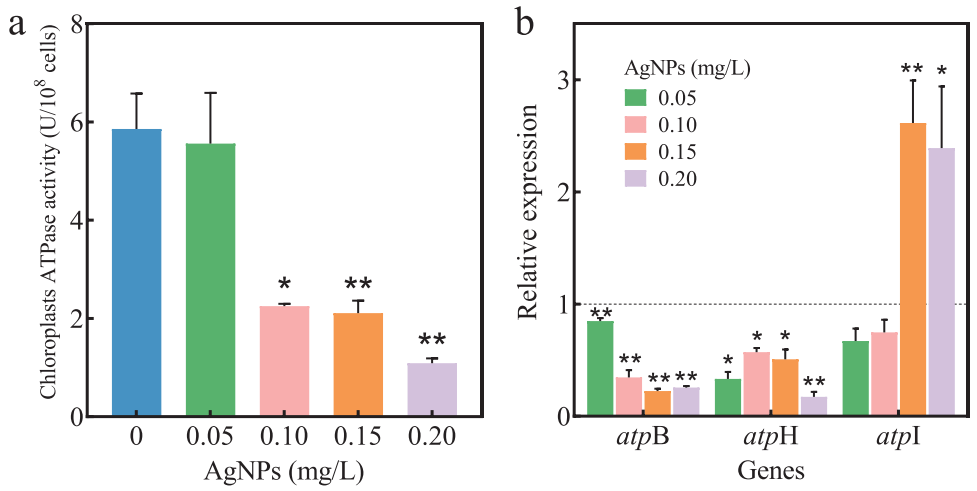

Fig. 2 – The variations of chloroplast ATPase activity (a) and expressions of ATPase-coding genes (b) in *C. vulgaris* under AgNPs stress. Data were expressed as mean ± SD ($n = 3$). * and ** indicate that the values are significantly different compared with the control group ($p < 0.05$ and $p < 0.01$, respectively).

ordered and rearranged along with disintegrated chloroplasts under AgNPs stress. The analysis of ROS level and MDA content also implied that the AgNPs caused oxidative damage to the thylakoid membranes (Appendix A **Fig. S5**). Notably, the thylakoid membrane is the carrier of photosynthetic protein complex as ATPase (Liu et al., 2020a). As a result, the structural destruction in the thylakoid membrane may affect the ATPase activity, thereby disturbing the photophosphorylation. The results from **Fig. 2a** showed that AgNPs significantly inhibited the chloroplast ATPase activity ($p < 0.05$). Specifically, the ATPase activity decreased by 81.4% of the control under 0.20 mg/L AgNPs stress. Spearman correlation analysis results from Appendix A **Fig. S6** showed that chloroplast ATPase activity was significantly and positively correlated with the ATP content of the algal cells (Spearman's correlation coefficient $r = 0.906$, $p < 0.05$). Thus, the suppression of chloroplast ATPase activity might have led to the blockage of energy supply. Similar to our results, TiO_2 NPs limited the ATPase activity along with low production of ATP and glucose, disrupting the energy metabolisms in algal photosynthesis (Middepogu et al., 2018).

Expressions of chloroplast ATPase-coding genes. Enzyme activity is highly regulated at a number of different levels, such as gene expression and translation. Accordingly, this study determined the expressions of key genes encoding chloroplast ATPase, including *atp*B, *atp*H, and *atp*I, after the algae were exposed to AgNPs. The result showed that AgNPs induced significant changes in the expression of these genes (**Fig. 2b**). After exposure to 0.20 mg/L AgNPs, the expression levels of *atp*B and *atp*H sharply decreased by 74.5% and 82.8% of the control ($p < 0.05$), respectively. These results are in agreement with the decrease in chloroplast ATPase activity. Our study implied that the downregulation of ATPase-coding genes *atp*B and *atp*H was one of the primary reasons for reduced ATP production. However, the gene *atp*I was remarkably upregulated after exposure to higher concentrations of AgNPs. In detail, the expression level of *atp*I increased by 161% under 0.15 mg/L AgNPs stress ($p < 0.05$), indicating a protection strategy of energy supply for algal cells responding to AgNPs attack.

Interactions of AgNPs and ATPase subunit. It was reported that AgNPs can be internalized into algal cells (Liu et al., 2020b). AgNPs in the cells may competitively bind with enzymes or alter their structure, causing the attenuation of enzyme activity (Mishra et al., 2021). However, it remains unknown if AgNPs can reduce ATPase activity by directly altering its structure, occupying the binding sites of substrates, or binding with substrates. To address this, we performed molecular docking to explore the binding of AgNPs and ATPase subunits. Among them, AgNPs had a strong binding affinity to AtpB according to shape complementarity principles (Appendix A **Table S3**). Moreover, the catalytic sites producing ATP from ADP and Pi are hosted primarily by AtpB. Therefore, we selected AtpB as a model protein to predict the interactions between AgNPs and ATPase. The results of docking simulation showed that the energy level of the simulated complex by AgNPs and AtpB ($E_{Total} = -1754$ kJ/mol) was lower than that of substrate ADP ($E_{Total} = -643$ kJ/mol) and Pi ($E_{Total} = -274$ kJ/mol), indicating more significant interaction between AgNPs and AtpB (Appendix A **Fig. S7**). Considering the contribution of chemical element of AgNPs, the docking simulation of interactions between Ag^+ and AtpB or substrates was also performed. Similarly, a more significant interaction between Ag^+ and AtpB was observed than interactions between Ag^+ and substrates (Appendix A **Fig. S7**). Moreover, AgNPs were more likely to bind to AtpB than Ag^+ according to the energy level of the simulated complex. Accordingly, the interaction mechanism between AgNPs and AtpB was further conducted.

Since ADP and Pi binding to the enzyme leads to the release of ATP from ATPase (Igamberdiev and Kleczkowski, 2015), we first observed the binding modes of ADP and Pi to AtpB. The results in Appendix A **Fig. S8** showed that multiple amino acid residues in the internal active cavity of AtpB were responsible for binding with ADP (TYR34, GLN56, GLN57, ARG281, THR291, THR294, and GLU295) and Pi (GLN56, PRO233, GLY234, ARG281, and LEU292). Hydrogen-bond and hydrophobic inter-

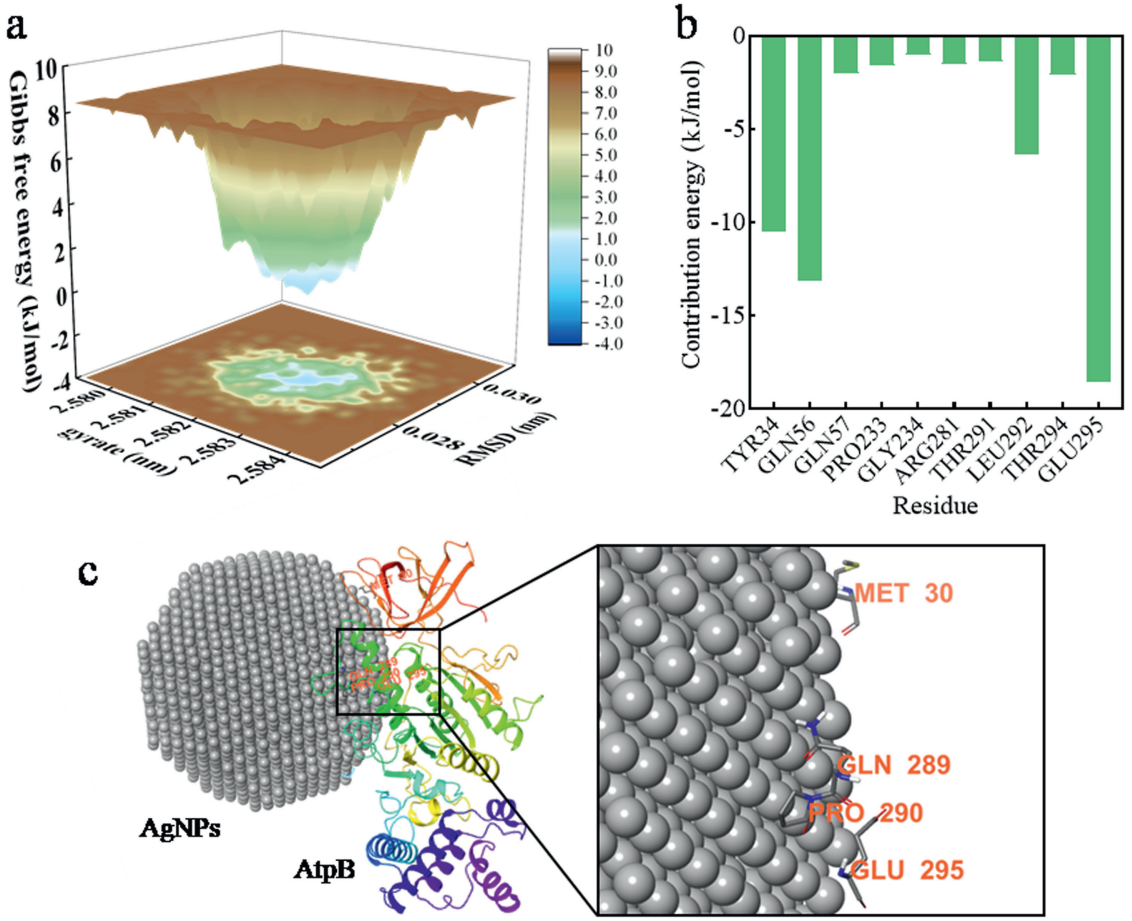

Fig. 3 – Molecular dynamics simulation between AgNPs and the ATPase. Free energy landscape (FEL) of the AgNPs-AtpB complex during the molecular dynamics simulation (a). The FEL with smaller energy zones (blue) and more concentrated brown regions suggested that the complex has greater stability. Binding energy distribution of the key residues of AtpB binding with AgNPs (b). These key residues overlap with the identified binding sites of AtpB and substrates ADP and Pi. Three-dimensional docking conformation of complex (c).

actions were the primary binding forces. In particular, ADP formed four hydrogen bonds with GLN57 (2.66 and 2.73 Å), ARG281 (2.71 Å), and TYR34 (2.89 Å). Pi formed two hydrogen bonds with ARG281 (2.58 Å) and GLN56 (2.59 Å). To further understand the effect of AgNPs on the binding sites of ADP and Pi to AtpB, molecular dynamics simulation was conducted to investigate the interaction between AgNPs and ATPase. As shown in **Fig. 3a** and Appendix A **Fig. S9**, root mean square deviation (RMSD) and radius of gyration (Rg) were maintained within the acceptable calculation range of 0-5 nsec, showing that the stable complex of AgNPs and AtpB might cause changes in the structure of AtpB. In detail, the key residues binding with AgNPs, such as MET30, GLN289, PRO290, and GLU295, contributed to producing the stable complex (**Fig. 3**). Notably, the binding sites between AgNPs and AtpB overlap with the identified binding sites of ADP or Pi and AtpB, such as TYR34 and GLN56 (**Fig. 3b**). In brief, AgNPs competed with substrates ADP and Pi for binding sites by forming a stable complex with AtpB, which may result in the inability of ADP and Pi to bind with AtpB so that ATP production was inhibited (**Fig. 1**).

2.3. *ATP-involving metabolic disturbances under AgNPs stress*

Insufficient energy supply caused by ATP reduction will be likely to disorder relevant metabolism. For this, the metabolic profiling disturbed by AgNPs was further investigated. In total, 69 metabolites were identified through an untargeted GC/TOF-MS-based metabolomics analysis (Appendix A **Fig. S10** and **Table S4**). Apparently, the higher concentration of the AgNPs-treated group and the control group showed more significant discrimination in volcano plots (Appendix A **Fig. S11**). Furthermore, PLS-DA was performed to draw a comparison of metabolic differences and similarities. The PLS-DA score plot showed significant separation between the 0.20 mg/L AgNPs-treated group and the control group along with component 1 (27.8%, Appendix A **Fig. S12**). These findings indicated that AgNPs induced global metabolic reprogramming in the algal cells. To obtain differential metabolites between the control group and the AgNPs-treated group, ANOVA and t-test were performed. Based on the VIP scores and one-way ANOVA (VIP > 1 and $p < 0.05$), 25 metabolites were significantly disturbed

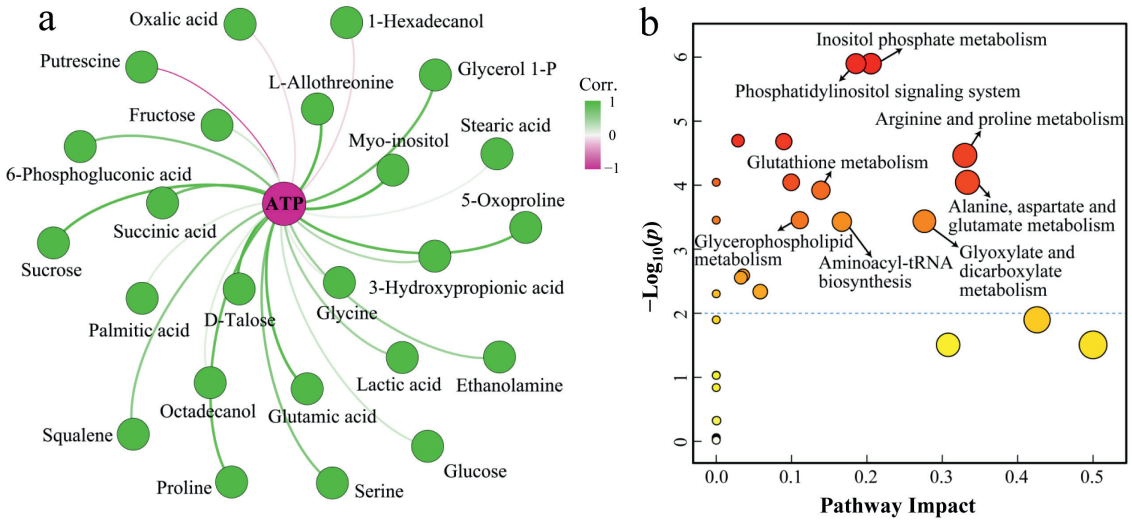

Fig. 4 – Metabolic analysis of *C. vulgaris* under AgNPs stress. Network analysis revealing the correlation between differential metabolites and ATP (a). Positive and negative correlations are indicated in green and pink lines, respectively. Analysis of metabolic pathway of the algal cells under AgNPs stress (b). A dot in the figure represents a metabolic pathway. The size of the dots shows the degree of influence. The color of the dots shows the *p*-value of influence (the more significant influence is redder).

after exposure to AgNPs. The metabolic correlation network was constructed according to the correlation between contents of these differential metabolites and ATP content. As shown in **Fig. 4a**, ATP content existed a significant positive correlation with the content of D-talose ($r = 0.879$, $p < 0.05$), myo-inositol ($r = 0.866$, $p < 0.05$), and L-allothreonine ($r = 0.826$, $p < 0.05$), etc., while a significantly negative correlation with putrescine content ($r = -0.826$, $p < 0.05$). The reduction of ATP content was accompanied by the decreased relative abundances of most differential metabolites. As can be seen, AgNPs induced significant disturbances in metabolites by blocking the energy supply by ATP.

To understand the functions of the differential metabolites, the relevant metabolic pathways were further conducted. As shown in **Fig. 4b**, eight metabolic pathways were remarkably disturbed upon exposure to AgNPs. Interestingly, most of these disturbed metabolic pathways were mediated by ATP. Therein, inositol phosphate metabolism, phosphatidylinositol signaling system, glycerophospholipid metabolism, aminoacyl-tRNA biosynthesis, and glutathione metabolism required ATP involvement.

The significant disturbances of the ATP-involving metabolic pathways suggested that AgNPs posed detrimental effects on the distribution and contents of relevant metabolites in algal cells. As shown in **Fig. 5**, the levels of myo-inositol and glucose 6-phosphate remarkably decreased by 57.6% and 21.2% of the control under 0.20 mg/L AgNPs stress, indicating the inhibition of inositol phosphate metabolism and phosphatidylinositol signaling system of algal cells. The results were consistent with our previous study that AgNPs also suppressed these two metabolic pathways of algal cells in the high-phosphorus condition (Qu et al., 2021). It has been found that myo-inositol can be converted into phosphatidylinositol. This product will be further phosphorylated to 1-phosphatidyl-1D-myo-inositol 3-phosphate by ATP and ultimately to phytate (Azevedo and Saiardi, 2017). The downregulation of myo-inositol reflected a negative regulatory process in which AgNPs possibly cut down the phosphorylation of phosphatidylinositol in the algal cells. Besides, as can be seen from the decreased glucose 6-phosphate content and the increased glucose content, AgNPs prevented ATP from providing phosphate groups and energy to glucose in these pathways. Similarly, the level of ethanolamine and glycerol 1-phosphate involved in glycerophospholipid metabolism decreased by 26.2% and 21.2% under 0.20 mg/L AgNPs stress (**Fig. 5**). This indicated that AgNPs destroyed the ATP-dependent phosphorylation of ethanolamine (Nakamura, 2017). The inhibition of phospholipid metabolisms exacerbated the membrane damage by AgNPs. For aminoacyl-tRNA biosynthesis, most of the detected amino acids, including serine, glutamic acid, and proline, were reduced in the algal cells in response to AgNPs stress (**Fig. 5**). Generally, these amino acids are stimulated in an ATP-dependent manner, and then transferred onto the 3′ terminal adenosine of the tRNA to form aminoacyl-tRNA (Sheppard et al., 2008). The current study also proved that AgNPs inhibited the aminoacyl-tRNA biosynthesis, thereby disturbing the protein translation process. Aside from these alterations, the levels of 5-oxoproline and glutamic acid remarkably decreased by 40.8% and 35.8% under 0.20 mg/L AgNPs stress. As the raw materials for glutathione metabolism, 5-oxoproline and glutamic acid were stimulated by ATP-dependent phosphorylation to synthesize glutathione (Li et al., 2022). Glutathione is considered a critical cellular antioxidant and a detoxification agent in cellular defense systems (Ouyang et al., 2018; Xu et al.,

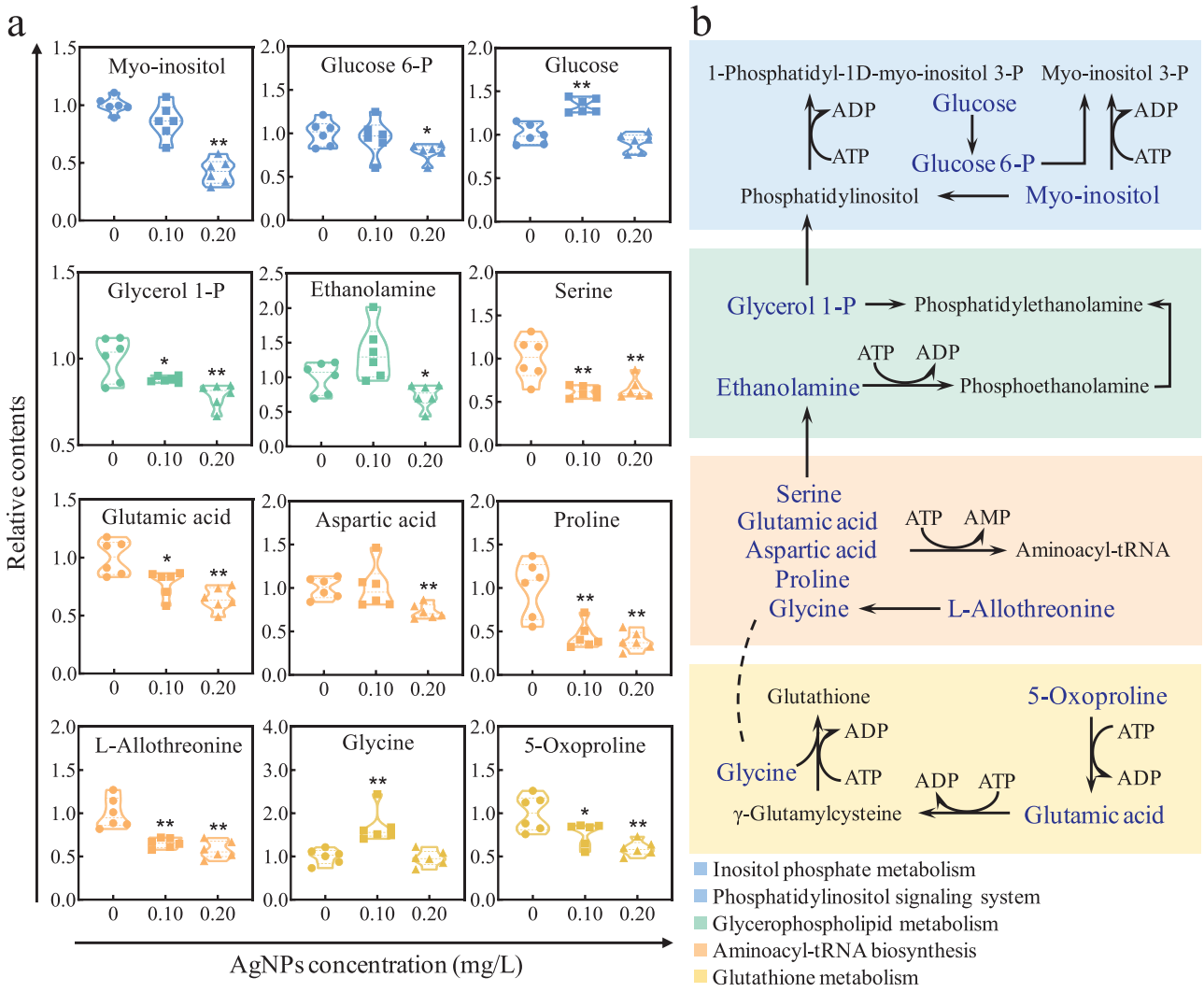

Fig. 5 – Disturbances of metabolic pathways mediated by ATP in *C. vulgaris* under AgNPs stress. Box plots of key metabolites in five metabolic pathways, including inositol phosphate metabolism, phosphatidylinositol signaling system, glycerophospholipid metabolism, aminoacyl-tRNA biosynthesis, and glutathione metabolism (a). The metabolite intensity values in the AgNPs-treated groups were normalized by those in the control groups. * and ** indicate that the values are significantly different compared with the control group ($p < 0.05$ and $p < 0.01$). Summary scheme showing the regulated metabolic pathways of the algal cells (b).

2022). The inhibition of glutathione metabolism in our study implied the inactivation of defense systems. Apparently, all these suppressed metabolic pathways are closely related to decreased ATP. As is well known, ATP is the primary energy carrier connecting anabolism and catabolism (Morciano et al., 2017). It has been demonstrated that the hindered ATP supply *in vivo* caused metabolic disturbances at the metabolomic and transcriptomic levels under abiotic stresses (Gao et al., 2020; Li et al., 2021). For instance, antibiotic stress inhibited the ATP supply in algae *Raphidocelis subcapitata*, thereby causing the suppression of DNA replication-coupled repair (Li et al., 2021). Overall, the blockage of energy supply due to the inhibited ATP generation was responsible for metabolic disturbances, ultimately inhibiting algal growth.

3. Conclusions

This study elucidated the mechanism of ATP reduction and relevant metabolic disturbances in algae triggered by AgNPs. Results confirmed that AgNPs decreased ATP production, which was attributed to the reduction of chloroplast ATPase activity and downregulation of its encoding genes *atp*B and *atp*H in the chloroplast. Furthermore, AgNPs can competitively bind to the active sites of AtpB by forming a stable complex with AtpB, potentially causing the inability of substrates to bind with AtpB. Metabolomics analysis revealed that AgNPs downregulated the ATP-involving metabolic pathways, including inositol phosphate metabolism, phosphatidylinositol signaling system, glycerophospholipid metabolism, aminoacyl-tRNA biosynthesis, and glutathione metabolism.

The perturbed metabolic pathways directly influenced the algal growth. These findings provided new insights into understanding the molecular mechanism of energy supply to regulate the metabolism of aquatic organisms under NPs stress.

Declaration of Competing Interest

The authors declare that they have no known competing financial interests or personal relationships that could have appeared to influence the work reported in this article.

Acknowledgments

This work was supported by the National Natural Science Foundation of China (Nos. 21577117 and 22076160) and the Postgraduate Scientific Research Innovation Project of Hunan Province (No. CX20210521). We thank Hunan Lihero Technology Co., LTD. (Changsha, China) for providing the experimental instrument.

Appendix A Supplementary data

Supplementary material associated with this article can be found, in the online version, at doi:10.1016/j.jes.2022.10.029.

REFERENCES

Azevedo, C., Saiardi, A., 2017. Eukaryotic phosphate homeostasis: The inositol pyrophosphate perspective. Trends Biochem. Sci. 42 (3), 219–231.

Berendsen, H.J.C., Van Der Spoel, D., Van Drunen, R., 1995. GROMACS: A message-passing parallel molecular dynamics implementation. Comput. Phys. Commun. 91 (1), 43–56.

Cao, M.M., Huang, X.T., Wang, F., Zhang, Y.Y., Zhou, B.H., Chen, H.L., et al., 2021. Transcriptomics and metabolomics revealed the biological response of *Chlorella pyrenoidesa* to single and repeated exposures of AgNPs at different concentrations. Environ. Sci. Technol. 55 (23), 15776–15787.

Carretero-González, R., Kevrekidis, P.G., Kevrekidis, I.G., Maroudas, D., Frantzeskakis, D.J., 2005. A Parrinello–Rahman approach to vortex lattices. Phys. Lett. A 341 (1-4), 128–134.

Chen, B., Li, F., Liu, N., Ge, F., Xiao, H.X., Yang, Y.X., 2015a. Role of extracellular polymeric substances from *Chlorella vulgaris* in the removal of ammonium and orthophosphate under the stress of cadmium. Bioresour. Technol. 190, 299–306.

Chen, H., Hu, J.L., Qiao, Y.Q., Chen, W.X., Rong, J.F., Zhang, Y.M., et al., 2015b. Ca^{2+}-regulated cyclic electron flow supplies ATP for nitrogen starvation-induced lipid biosynthesis in green alga. Sci. Rep. 5 (1), 15117.

Chen, Z.Y., Gao, S.H., Jin, M., Sun, S.J., Lu, J., Yang, P., et al., 2019. Physiological and transcriptomic analyses reveal CuO nanoparticle inhibition of anabolic and catabolic activities of sulfate-reducing bacterium. Environ. Int. 125, 65–74.

Chu, F.F., Cheng, J., Li, K., Wang, Y.G., Li, X., Yang, W.J., 2020. Enhanced lipid accumulation through a regulated metabolic pathway of phosphorus luxury uptake in the microalga *Chlorella vulgaris* under nitrogen starvation and phosphorus repletion. ACS Sustain. Chem. Eng. 8 (22), 8137–8147.

Costa, C.H.D., Perreault, F., Oukarroum, A., Melegari, S.P., Popovic, R., Matias, W.G., 2016. Effect of chromium oxide (III) nanoparticles on the production of reactive oxygen species and photosystem II activity in the green alga *Chlamydomonas reinhardtii*. Sci. Total Environ. 565, 951–960.

Gao, X., Deng, R., Lin, D.H., 2020. Insights into the regulation mechanisms of algal extracellular polymeric substances secretion upon the exposures to anatase and rutile TiO_2 nanoparticles. Environ. Pollut. 263, 114608.

Grün, A.L., Straskraba, S., Schulz, S., Schloter, M., Emmerling, C., 2018. Long-term effects of environmentally relevant concentrations of silver nanoparticles on microbial biomass, enzyme activity, and functional genes involved in the nitrogen cycle of loamy soil. J. Environ. Sci. 69, 12–22.

Guo, X.R., Yin, Y.G., Tan, Z.Q., Liu, J.F., 2018. Environmentally relevant freeze–thaw cycles enhance the redox-mediated morphological changes of silver nanoparticles. Environ. Sci. Technol. 52 (12), 6928–6935.

Huang, B., Wei, Z.B., Yang, L.Y., Pan, K., Miao, A.J., 2019. Combined toxicity of silver nanoparticles with hematite or plastic nanoparticles toward two freshwater algae. Environ. Sci. Technol. 53 (7), 3871–3879.

Huang, M., Keller, A.A., Wang, X.M., Tian, L.Y., Wu, B., Ji, R., et al., 2020. Low concentrations of silver nanoparticles and silver ions perturb the antioxidant defense system and nitrogen metabolism in N_2-fixing cyanobacteria. Environ. Sci. Technol. 54 (24), 15996–16005.

Igamberdiev, A.U., Kleczkowski, L.A., 2015. Optimization of ATP synthase function in mitochondria and chloroplasts via the adenylate kinase equilibrium. Front. Plant Sci. 6, 10.

Jin, X.T., Su, H.L., Ding, G.B., Sun, Z.D., Li, Z.Y., 2019. Exposure to ambient fine particles causes abnormal energy metabolism and ATP decrease in lung tissues. Chemosphere 224, 29–38.

Li, M., Ruan, L.Y., Dang, F., Liu, H.L., Zhou, D.M., Yin, B., et al., 2022. Metabolic response of earthworms (*Pheretima guillemi*) to silver nanoparticles in sludge-amended soil. Environ. Pollut. 300, 118954.

Li, Q., Lu, D.L., Sun, H.T., Guo, J.H., Mo, J.Z., 2021. Tylosin toxicity in the alga *Raphidocelis subcapitata* revealed by integrated analyses of transcriptome and metabolome: Photosynthesis and DNA replication-coupled repair. Aquat. Toxicol. 239, 105964.

Liang, B.X., Huang, Y.J., Zhong, Y.Z., Li, Z.M., Ye, R.Y., Wang, B., et al., 2022. Brain single-nucleus transcriptomics highlights that polystyrene nanoplastics potentially induce Parkinson's disease-like neurodegeneration by causing energy metabolism disorders in mice. J. Hazard Mater. 430, 128459.

Liang, C.J., Zhang, B.J., 2018. Effect of exogenous calcium on growth, nutrients uptake and plasma membrane H^+-ATPase and Ca^{2+}-ATPase activities in soybean (*Glycine max*) seedlings under simulated acid rain stress. Ecotox. Environ. Safe. 165, 261–269.

Liu, N., Lin, F.J., Chen, J., Shao, Z.X., Zhang, X.R., Zhu, L.Z., 2021. Multistage defense system activated by tetrachlorobiphenyl and its hydroxylated and methoxylated derivatives in *Oryza sativa*. Environ. Sci. Technol. 55 (8), 4889–4898.

Liu, N., Wang, Y.P., Ge, F., Liu, S.X., Xiao, H.X., 2018. Antagonistic effect of nano-ZnO and cetyltrimethyl ammonium chloride on the growth of *Chlorella vulgaris*: Dissolution and accumulation of nano-ZnO. Chemosphere 196, 566–574.

Liu, N., Zhang, H., Zhao, J.F., Xu, Y., Ge, F., 2020a. Mechanisms of cetyltrimethyl ammonium chloride-induced toxicity to photosystem II oxygen evolution complex of *Chlorella vulgaris* F1068. J. Hazard Mater. 383, 121063.

Liu, N., Zhu, L.Z., 2020. Metabolomic and transcriptomic investigation of metabolic perturbations in *Oryza sativa* L. triggered by three pesticides. Environ. Sci. Technol. 54 (10), 6115–6124.

Liu, W., Majumdar, S., Li, W.W., Keller, A.A., Slaveykova, V.I., 2020b. Metabolomics for early detection of stress in freshwater alga *Poterioochromonas malhamensis* exposed to silver nanoparticles. Sci. Rep. 10 (1), 20563.

Liu, Y., Chen, S., Chen, X., Zhang, J., Gao, B.Y., 2015. Interactions between *Microcystis aeruginosa* and coexisting amoxicillin contaminant at different phosphorus levels. J. Hazard. Mater. 297, 83–91.

Luo, S.W., Alimujiang, A., Balamurugan, S., Zheng, J.W., Wang, X., Yang, W.D., et al., 2021. Physiological and molecular responses in halotolerant *Dunaliella salina* exposed to molybdenum disulfide nanoparticles. J. Hazard. Mater. 404, 124014.

Marisa, I., Asnicar, D., Matozzo, V., Parolini, M., Brianese, N., Fedorova, M., et al., 2022. Zinc oxide, titanium dioxide and C_{60} fullerene nanoparticles, alone and in mixture, differently affect biomarker responses and proteome in the clam *Ruditapes philippinarum*. Sci. Total Environ. 838, 155873.

Matich, E.K., Chavez Soria, N.G., Aga, D.S., Atilla-Gokcumen, G.E., 2019. Applications of metabolomics in assessing ecological effects of emerging contaminants and pollutants on plants. J. Hazard. Mater. 373, 527–535.

Middepogu, A., Hou, J., Gao, X., Lin, D.H., 2018. Effect and mechanism of TiO_2 nanoparticles on the photosynthesis of *Chlorella pyrenoidosa*. Ecotox. Environ. Safe. 161, 497–506.

Mishra, S., Wang, W.T., de Oliveira, I.P., Atapattu, A.J., Xia, S.W., Grillo, R.T., et al., 2021. Interaction mechanism of plant-based nanoarchitectured materials with digestive enzymes of termites as target for pest control: Evidence from molecular docking simulation and in vitro studies. J. Hazard. Mater. 403, 123840.

Mo, J.Z., Ma, Z.H., Yan, S.W., Cheung, N.K.M., Yang, F.S., Yao, X.N., et al., 2023. Metabolomic profiles in a green alga (*Raphidocelis subcapitata*) following erythromycin treatment: ABC transporters and energy metabolism. J. Environ. Sci. 124, 591–601.

Morciano, G., Sarti, A.C., Marchi, S., Missiroli, S., Falzoni, S., Raffaghello, L., et al., 2017. Use of luciferase probes to measure ATP in living cells and animals. Nat. Protoc. 12 (8), 1542–1562.

Nakamura, Y., 2017. Plant phospholipid diversity: Emerging functions in metabolism and protein–lipid interactions. Trends Plant Sci 22 (12), 1027–1040.

Nam, S.H., Il Kwak, J., An, Y.J., 2018. Quantification of silver nanoparticle toxicity to algae in soil via photosynthetic and flow-cytometric analyses. Sci. Rep. 8 (1), 292.

OECD, 2006. OECD guidelines for the testing of chemicals No. 201: Freshwater Alga and Cyanobacteria, Biomass Inhibition Test. Organization for Economic Cooperation and Development, Paris.

Ouyang, S.H., Hu, X.G., Zhou, Q.X., Li, X.K., Miao, X.Y., Zhou, R.R., 2018. Nanocolloids in natural water: Isolation, characterization, and toxicity. Environ. Sci. Technol. 52 (8), 4850–4860.

Qi, Q.J., Li, Q., Li, J., Mo, J.Z., Tian, Y.L., Guo, J.H., 2022 . Transcriptomic analysis and transgenerational effects of ZnO nanoparticles on *Daphnia magna*: Endocrine-disrupting potential and energy metabolism. Chemosphere 290, 133362.

Qu, R.H., Xie, Q.T., Tian, J., Zhou, M., Ge, F., 2021. Metabolomics reveals the inhibition on phosphorus assimilation in *Chlorella vulgaris* F1068 exposed to AgNPs. Sci. Total Environ. 770, 145362.

Schneidman-Duhovny, D., Inbar, Y., Nussinov, R., Wolfson, H.J., 2005. PatchDock and SymmDock: Servers for rigid and symmetric docking. Nucleic Acids Res 33, W363–W367.

Sheppard, K., Yuan, J., Hohn, M.J., Jester, B., Devine, K.M., Söll, D., 2008. From one amino acid to another: tRNA-dependent amino acid biosynthesis. Nucleic Acids Res 36 (6), 1813–1825.

Tao, Y., Yang, Y., Jiao, Y.Q., Wu, S., Zhu, G.X., Akindolie, M.S., et al., 2020. Monobutyl phthalate (MBP) induces energy metabolism disturbances in the gills of adult zebrafish (*Danio rerio)*. Environ. Pollut. 266, 115288.

Wang, P., Zhang, B., Zhang, H., He, Y.L., Ong, C.N., Yang, J., 2019. Metabolites change of *Scenedesmus obliquus* exerted by AgNPs. J. Environ. Sci. 76, 310–318.

Wang, X.H., Qin, Y.J., Li, X.Y., Yan, B., Martyniuk, C.J., 2021. Comprehensive interrogation of metabolic and bioenergetic responses of early-staged zebrafish (*Danio rerio*) to a commercial copper hydroxide nanopesticide. Environ. Sci. Technol. 55 (19), 13033–13044.

Wu, J.K., Zhan, M.J., Chang, Y., Su, Q.X., Yu, R., 2018. Adaption and recovery of *Nitrosomonas europaea* to chronic TiO_2 nanoparticle exposure. Water Res. 147, 429–439.

Xie, Q.T., Gu, R.M., Lin, D.H., Liu, N., Qu, R.H., Ge, F., 2022. *In situ* assay of interfacial interaction between ZnO nanoparticles and live cell disturbed by surfactants. Environ. Sci. Technol. 56 (18), 13066–13075.

Xie, Q.T., Liu, N., Lin, D.H., Qu, R.H., Zhou, Q.Z., Ge, F., 2020. The complexation with proteins in extracellular polymeric substances alleviates the toxicity of Cd (II) to *Chlorella vulgaris*. Environ. Pollut. 263, 114102.

Xu, L.M., Zhao, Z.L., Yan, Z., Zhou, G.X., Zhang, W.M., Wang, Y., et al., 2022. Defense pathways of *Chlamydomonas reinhardtii* under silver nanoparticle stress: Extracellular biosorption, internalization and antioxidant genes. Chemosphere 291, 132764.

Zhang, H., Liu, N., Zhao, J.F., Ge, F., Xu, Y., Chen, Y.H., 2019. Disturbance of photosystem II-oxygen evolution complex induced the oxidative damage in *Chlorella vulgaris* under the stress of cetyltrimethylammonium chloride. Chemosphere 223, 659–667.

Zhang, J.L., Shen, L., Xiang, Q.Q., Ling, J., Zhou, C.H., Hu, J.M., et al., 2020a. Proteomics reveals surface electrical property-dependent toxic mechanisms of silver nanoparticles in *Chlorella vulgaris*. Environ. Pollut. 265, 114743.

Zhang, Y.D., Liu, N., Wang, W., Sun, J.T., Zhu, L.Z., 2020b. Photosynthesis and related metabolic mechanism of promoted rice (*Oryza sativa* L.) growth by TiO_2 nanoparticles. Front. Environ. Sci. Eng. 14 (6), 103.

Zhao, J.F., Liu, S.X., Liu, N., Zhang, H., Zhou, Q.Z., Ge, F., 2019. Accelerated productions and physicochemical characterizations of different extracellular polymeric substances from *Chlorella vulgaris* with nano-ZnO. Sci. Total Environ. 658, 582–589.

Zhong, X., Downs, C.A., Che, X.K., Zhang, Z.S., Li, Y.M., Liu, B.B., et al., 2019. The toxicological effects of oxybenzone, an active ingredient in suncream personal care products, on prokaryotic alga *Arthrospira* sp. and eukaryotic alga *Chlorella* sp. Aquat. Toxicol. 216, 105295.

Zhou, Q.Z., Li, F., Ge, F., Liu, N., Kuang, Y.D., 2016. Nutrient removal by *Chlorella vulgaris* F1068 under cetyltrimethyl ammonium bromide induced hormesis. Environ. Sci. Pollut. Res. Int. 23 (19), 19450–19460.